Finanziato dall'Unione europea
NextGenerationEU

Ministero dell'Università e della Ricerca

Global Stability of Road Vehicle Motion - STAVE

Deliverable 1
Vehicle and Driver Models for Stability Studies

Document in fulfilment of
MILESTONE 1
"Car and diver models ready"

This project has received funding from Italian Ministero del Merito e della Ricerca, PRIN: Progetti di ricerca di rilevante interesse nazionale – Bando 2022 PNRR Prot. P2022KSN9Z

Table of Contents

Abstract

This deliverable aims at producing the models that will be used in the subsequent WPs of the STAVE project. Models of different complexities of the car are derived and described. A deriver model, suited for stability analysis is produced. Preliminary experimental tests at the driving simulator and on the track are described.

This document is organized as follows.

Section 1 describes the vehicle models selected for the project. Five models have been selected, namely a complete fourteen-degree-of-freedom model, a simplified two-degree-of-freedom model, a simplified three-degree-of-freedom model, a simplified coupled longitudinal-lateral model, and a complete handwritten fourteen-degree-of-freedom model.

Section 2 is devoted to the description of the driver model. A driver model with a third-order delay has been selected as the more appropriate driver model for the project.

In Section 3, the control models employed in the project are described. In the section, the reference generator, the controller, and the wheel torque manager are explained.

Section 4 reports the experimental techniques for the measurement of the tyre characteristics and inertia properties of vehicles considered in the project.

The preliminary tests performed at the driving simulator and the comparison with tests performed on a track are reported in Section 5.

Section 6 provides the list of the published documents pertinent with the project.

Conclusions in Section 7.

1 Vehicle Models

This section is devoted to providing a concise description of the five models selected for the project.

1.1 Model 1 – Complete fourteen-degree-of-freedom model developed by commercial software (14dof-com model)

The complete fourteen-degree-of-freedom model has been developed by the commercial software VI-CarRealTime by Vi-Grade [1]. The model will be addressed as 14dof-com model in this deliverable and represents a Maserati Ghibli, has been validated by experimental tests, and the main data are reported in Table 1.

Table 1: Main parameters of the 14dof-com model.

Vehicle parameter	Value
Chassis mass	1691.4 kg
Chassis centre of gravity height	549.7 mm
Chassis moment of inertia	3341 kgm^2
Front wheel mass	52 kg
Rear wheel mass	40 kg
Vehicle mass	1938.4 kg
Vehicle centre of gravity height	537.3 mm
Vehicle moment of inertia	3992 kgm^2
Front axle distance from CG	1443.9 mm
Rear axle distance from CG	1529.1 mm
Wheelbase	2973.0 mm
Trackwidth, front	1628.0 mm
Trackwidth, rear	1636.0 mm
Steering ratio	14.31
Static toe angle, front (closed if positive)	-0.04167 deg
Static camber angle, front	-0.39167 deg
Static camber angle, rear	-0.98333 deg

The model features the vehicle body, modelled as a six DoFs rigid body, connected to the four wheels by suspensions described by lookup tables. The wheels are modelled by a rigid body comprising the mass of the hub and of the wheel with one DoF. For each wheel, a second DoF is considered to model the wheel rotation around its axis. The powertrain is modelled by means of lookup tables representing the characteristics of the engine and of the transmission. The differential unit is also included. Tyres are modelled by a PAC2002 model [2].

Two sets of vehicle parameters are considered, one called UN (understeering) and one called OV (oversteering). The two sets differ only for the following quantities.

- Static toe angle rear wheels (closed if positive): UN: +0.18333 deg; OV: -1 deg.
- Rear tires: UN: MERGE_p0_000.tir ; OV: MERGE_p1_000.tir.

The model is ready to be used at the driving simulator.

The model is available to all the researchers involved in the project in the project shared repository along with all pertinent data.

The model has been validated in previous activities between Politecnico di Milano and an industrial partner documented in published papers [3][4].

1.2 Model 2 – Simplified two-degree-of-freedom model (2dof model)

Referring to Figure 1, the equations of motion can be derived as follows. A moving reference system with origin fixed at the center of gravity of the vehicle is used. The longitudinal axis is parallel to the centerline of the vehicle; the vertical axis is perpendicular to the ground and directed towards the ground; the lateral axis is congruent with a right-hand reference system. The two degrees of freedom are the lateral motion yG and the yaw rotation ψ. The longitudinal motion is not considered as a degree of freedom and the longitudinal speed is considered constant. The longitudinal forces, either front or rear (F_{xi} $(i=f,r)$) are needed to keep constant the longitudinal speed; their magnitude is considered small and they are neglected. The lateral axle forces, either front or rear F_{yi} $(i=f,r)$ refer to the so called "Axle characteristics" [2] and can be modelled by using the well-known Pacejka Magic Formula [2] which was adapted and reads

$$F_{y_i}(\alpha_i) = D_i \sin\left(C_i \arctan\left(B_i\alpha_i - E_i(B_i\alpha_i - \arctan(B_i\alpha_i))\right)\right) \qquad i = f, r$$

Eq. 1

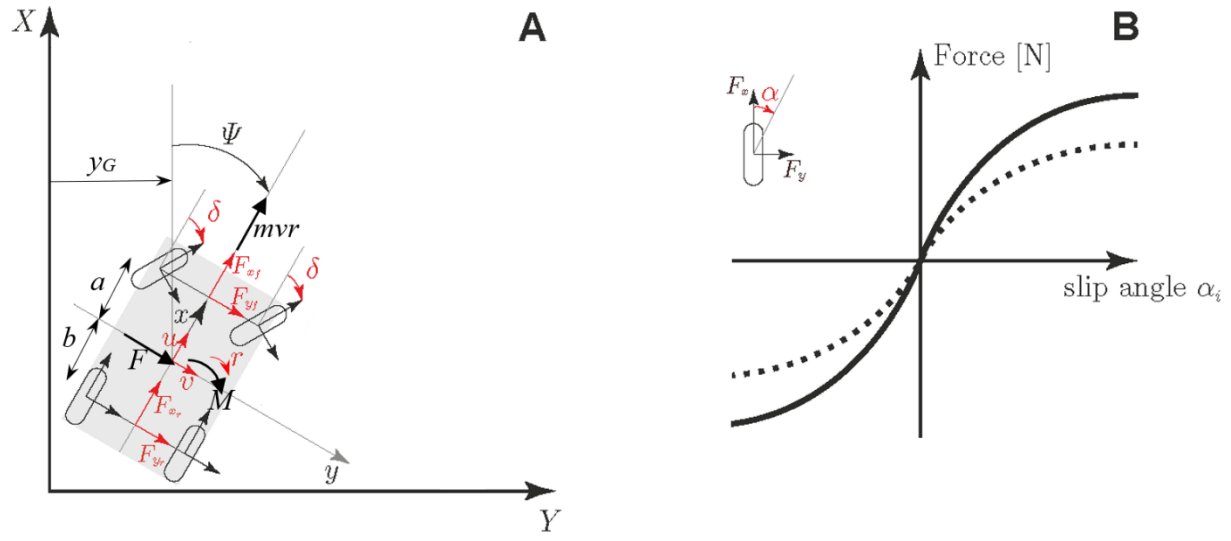

*Figure 1: 2dof model of a vehicle moving in the horizontal plane. (**A**) The forces acting at the four wheels are substituted by the resultants acting at the front and at the rear axle centers. The vehicle body is simply a rigid body moving in the XY plane. The mathematical model is defined by DoFs, namely y_G and ψ, with derivatives v and r. The steering angle δ is an imput of the model and can be used to connect a driver model. (**B**) Forces acting at the front (dotted line) or at the rear axle (solid line), depending on tire sideslip angle α_i (i=F,R)*

The total axle lateral force depends on the sideslip angle α_i, $(i=f,r)$ defined as small

$$\alpha_f = \delta - \left(\frac{v + ra}{u}\right)$$

Eq. 2

$$\alpha_r = -\left(\frac{v - rb}{u}\right)$$

Eq. 3

where the meaning of symbols can be taken from Figure 1. The equations of motion of the single-track model can be derived by using the D'Alembert principle and the following equations are derived

$$\dot{v} = \frac{1}{m}\left(F_{y_f} + F_{y_r}\right) - ur$$

Eq. 4

$$\dot{r} = \frac{1}{J}\left(aF_{y_f} - bF_{y_r}\right)$$

Eq. 5

The model is available to all the researchers involved in the project in the project shared repository along with all pertinent data.

1.2.1 Identification of the tyre parameters

The tyre parameters of the 2dof model have been identified on the basis of the parameters of the 14dof-com model by the following procedure.

a) A almost steady state steering pad manoeuvre has been simulated with the 14dof-com model. The manoeuvre has a velocity from 3 to 30 m/s, a radius of 80 m, and a duration of 27 s.

b) The normalized axle characteristics and the handling diagram have been computed from the simulated data. The load transfer due to the small longitudinal acceleration (below 0.1 m/s^2) has been neglected.

c) The simulation has been repeated for the UN and the OV vehicle.

d) The parameters of the tyre model of Eq. 1 have been identified to match the computed handling diagrams. In the identification, as the front tyres are the same for the two vehicles, these tyres have been identified simultaneously on the two diagrams and the parameters are the same for the two vehicles. The *D* parameter has been set equal to the product between the vertical load on the considered axis and the "Longitudinal friction Mux at Fznom" from the corresponding .tir file.

In Figure 2 the handling diagrams of the UN and OV vehicles obtained by the 14dof-com model and the 2dof model are compared. Table 2 reports the identified tyre parameters for the 2dof-model.

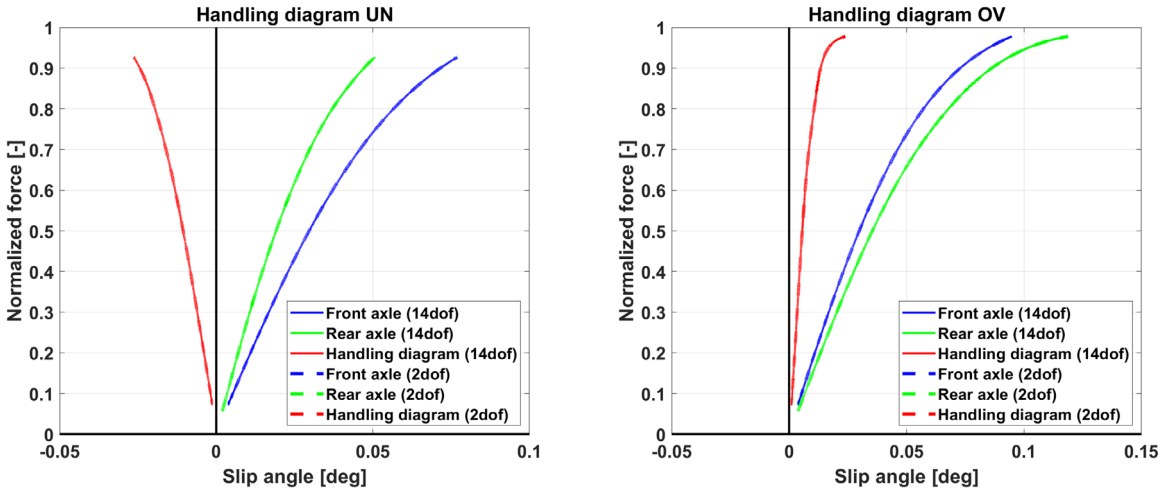

Figure 2: Handling diagrams for the UN and OV vehicles computed by the 14dof-com model and the 2dof model.

Table 2: Identified tyre parameters (parameters refer to the axle).

	B	C	D	E
Front tyres	9.14	1.85	10630 N	1.03
Rear tyres UN	17.14	1.37	11346 N	0.95
Rear tyres OV	7.53	1.87	10020 N	1.04

Track tests and some tests at the driving simulator are performed with the accelerator released. In this condition, the vehicle shows a deceleration of about 1 m/s^2. A load transfer is thus present between front and rear axles. Such load transfer is not modelled in the 2dof model. To represent this situation, the tyres parameters are identified by repeating the procedure where in the complete model a moment replicating the load transfer is applied during the steering pad maneuvre. Figure 3 and Table 3 report the results of the identification.

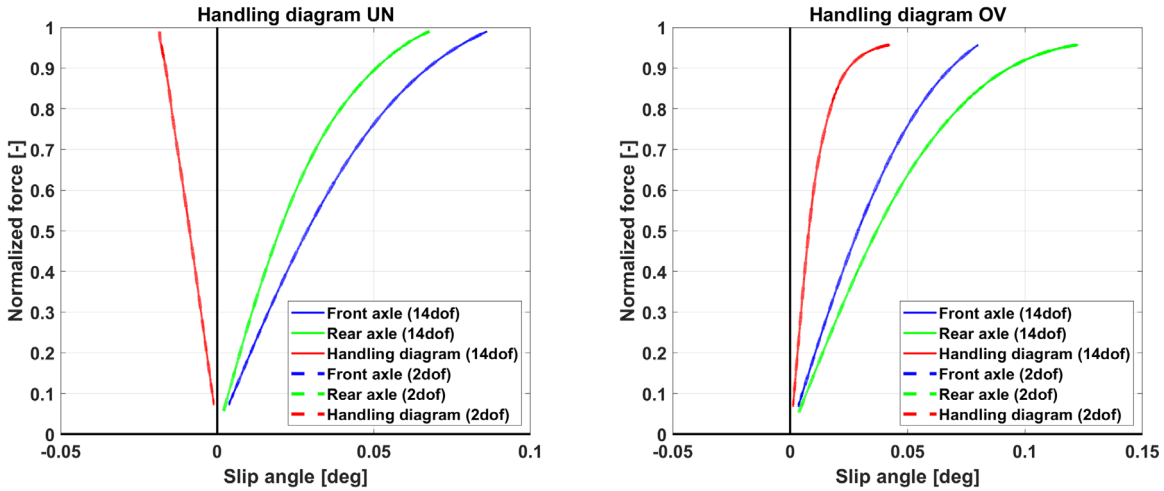

Figure 3: Handling diagrams for the UN and OV vehicles computed by the 14dof-com model and the 2dof model. Longitudinal deceleration of 1 m/s².

Table 3: Identified tyre parameters (parameters refer to the axle). Longitudinal deceleration of 1 m/s².

	B	C	D	E
Front tyres	9.25	1.82	10980 N	0.97
Rear tyres UN	17.31	1.35	10996 N	0.90
Rear tyres OV	7.32	1.93	9669 N	1.04

1.3 Model 3 – Simplified three-degree-of-freedom model (3dof model)

A three degrees of freedom model is implemented following the book "The Science of Vehicle Dynamics" of Professor Guiggiani. As depicted in Figure 4, the three degrees of freedom are the position of center of mass and the yaw angle ψ. A moving reference system with origin fixed at the center of gravity of the vehicle is used, as shown in Figure 5. The longitudinal axis is parallel to the centerline of the vehicle; the vertical axis is perpendicular to the ground and directed towards the ground; the lateral axis is congruent with a right-hand reference system.

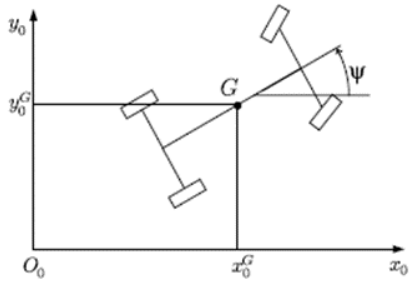

Figure 4: Ground-fixed coordinate system and yaw angle ψ.

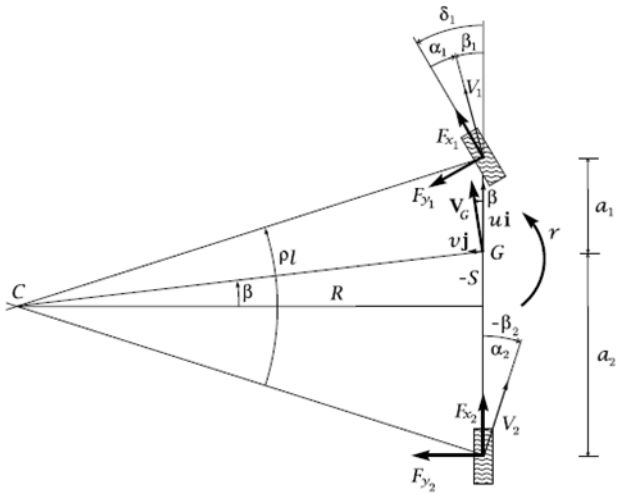

Figure 5: Single track model.

the complete system of six first-order ordinary differential equations is given by:

$$m\dot{u} = F_{x_1}\cos(\delta) + F_{x_2} - F_{y_1}\sin(\delta) - F_d \quad \text{(a)}$$

$$m\dot{v} = F_{y_1}\cos(\delta) + F_{y_2} + F_{x_1}\sin(\delta) \quad \text{(b)}$$

$$J_z\dot{r} = (F_{y_1}\cos(\delta) + F_{x_1}\sin(\delta))a_1 - F_{y_2}a_2 \quad \text{(c)}$$

$$\dot{x}_0^G = u\cos(\delta) - v\sin(\delta) \quad \text{(d)}$$

$$\dot{y}_0^G = u\sin(\delta) + v\cos(\delta) \quad \text{(e)}$$

$$\dot{\psi} = r \quad \text{(f)}$$

Eq. 6

Where δ is the steering angle of the front wheels, F_{x_i} and F_{y_i} (i = 1,2), are the longitudinal and lateral axle forces, respectively. Eq. 6a to Eq. 6c are the *equilibrium equations* along longitudinal, lateral and vertical directions, respectively, while Eq. 6d to Eq. 6f represent *kinematic reconstruction equations* for the yaw angle and for the coordinates of the vehicle's centre of mass G with respect to a fixed frame. Hence, m denotes the vehicle mass, J_z the vertical moment of inertia with respect to G, and a_1, a_2, the distance between G and the front and rear axles, respectively.

In Eq. 6a, $F_d = \rho S C_x u^2/2$ is the aerodynamic drag force, which is quadratic in the vehicle speed u and it is affected by the air density ρ, the frontal area S, and the drag coefficient C_x.

The vehicle data and parameters are the one used for the 2-dof model (sec. 1.2), indicating consistency also in the axle characteristics.

1.4 Model 4 – Simplified coupled longitudinal-lateral model

The most common implementation of vehicle dynamics control strategies exploits wheels longitudinal forces to generate an equivalent yaw torque, which is used as an additional (w.r.t. the driver steering wheel) vehicle input in order to modify its dynamics.

Other technological solutions may be employed for the same purpose (e.g. steer-by-wire, rear wheel drive, etc..) but refer to a-typical vehicle architectures. Thus at present they are not considered.

Given these premises, it is clear that in order to design and analyse vehicle dynamics control strategies it is crucial to account for the longitudinal – lateral vehicle dynamics coupling. To do so, the vehicle dynamics model presented in the following is considered.

The model is developed under the following assumptions:

1. Small steer angle.
2. Moderate sideslip angles.
3. Moderate load transfers, which in turn implies low lateral accelerations. This hypothesis is consistent, for example, with a low-grip scenario where the vehicle dynamics control systems are in fact meant to operate.
4. Symmetric (lef-right) vehicle geometry and parameters.
5. Identical tires parameters.

The model equations read as follows.

Force and torque balances

$$\dot{u} = \frac{1}{m}[F_{xfl} + F_{xfr} + F_{xrl} + F_{xrr}] + vr$$

Eq. 7

$$\dot{v} = \frac{1}{m}[F_{yfl} + F_{yfr} + F_{yrl} + F_{yrr}] - ur$$

Eq. 8

$$\dot{r} = \frac{1}{J}[l_f(F_{yfl} + F_{yfr}) - l_r(F_{yrl} + F_{yrr}) + p(F_{xfr} + F_{xrr}) - p(F_{xfl} + F_{xfr})]$$

Eq. 9

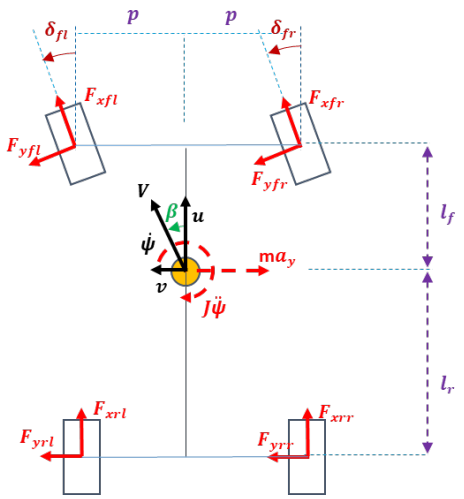

Figure 6: Couple longitudinal-lateral model.

Tire forces

$$\begin{aligned} F_{xi} &= f_x(\lambda_i, \alpha_i) \\ F_{yi} &= f_y(\lambda_i, \alpha_i) \end{aligned} \qquad i = fl, fr, rl, rr$$

Eq. 10

Where λ_i are the longitudinal tire slip and α_i the tire sideslip angles. They are defined as in the following section.

The functions $f_x(\lambda_i, \alpha_i)$ and $f_y(\lambda_i, \alpha_i)$ embed the well-known Pacejka Magic Formula [2] and consider the vertical load as a constant parameter (consistently with the previous hypothesis).

Kinematic relations

$$\begin{aligned} \lambda_i &= \frac{R_i \omega_i - u}{u} \\ \alpha_i &= \frac{v + r x_i}{u} - \delta_i \end{aligned} \qquad i = fl, fr, rl, rr$$

Eq. 11

Where ω_i are each wheel angular speed, R_i the corresponding nominal rolling radius, x_i is the longitudinal distance (with sign) of each wheel w.r.t the center of gravity of the vehicle. The symbol δ_i generally stands for the wheel steering angle (equal to the driver steer for the front and null for the rear wheels in case of standard 2 wheel steering vehicle).

Wheel dynamics

The torque balance of each wheel can be written see [8] in terms of the corresponding wheel slip, as follows:

$$\dot{\lambda}_i = -\frac{1}{u}\left[\frac{1-\lambda_i}{\tilde{m}_i} + \frac{R_i^2}{J_{wi}}\right] \cdot F_{xi}(\lambda_i, \alpha_i) + \frac{R_i}{u J_{wi}} T_i \qquad i = fl, fr, rl, rr$$

Eq. 12

Where T_i are the applied traction/braking wheel torque to each wheel, $\tilde{m}_i$ is the equivalent wheel and vehicle mass and J_{wi} the corresponding rolling inertia. It should be noted how each wheel is considered as independent from the others, as the mutual effect of a driving/braking torque on the non-corresponding wheel, despite not being analytically null, can be considered negligible.

1.5 Model 5 – Complete handwritten fourteen-degree-of-freedom model (14dof-hand model)

Bodies.

Our vehicle is modeled as an articulated system of rigid bodies. There are chassis, knuckles and wheels.

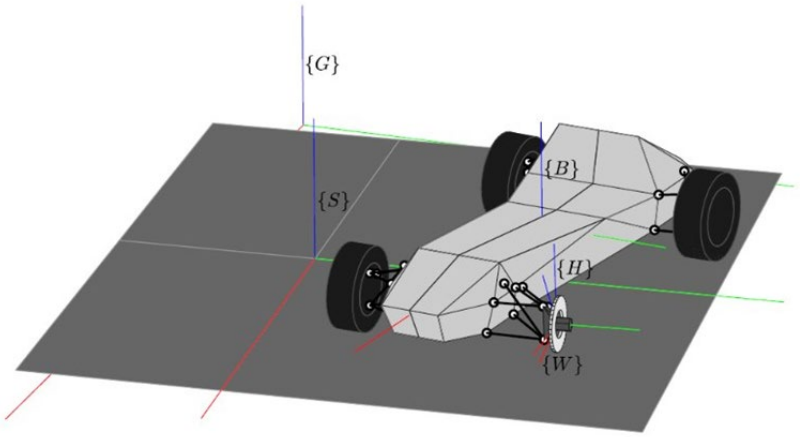

Figure 7: Constitutive bodies of the vehicle, and the respective reference frames

To keep track of the pose and motion of the frames, we attach a reference frame to each of them. We define two additional reference frames: one inertial frame, fixed to ground, and one moving frame, that follows the vehicle on track.

Joints.

After bodies and frames are established, we introduce joints between them. Joints limit the possible motion between the bodies they connect. After the introduction of joints, the vehicle and its constitutive parts will enjoy, in total, 14 degrees of freedom (DoF): 6 for the rigid body motion of the chassis, 4 for the suspensions (in particular, the spring deflection is used) and 4 for the rotation of the wheels.

Suspensions.

Suspensions are modeled as generalized 1-DoF joints. The configuration, as well as the motion subspace allowed by each suspension, is characterized in terms of a single scalar variable using a regression

procedure. This regression procedure is performed using the tabular data from CarRealTime, as shown in Figure 8.

The generalized force of the suspension joint is due to spring, damper, anti-roll bars, bumpers and rebounds.

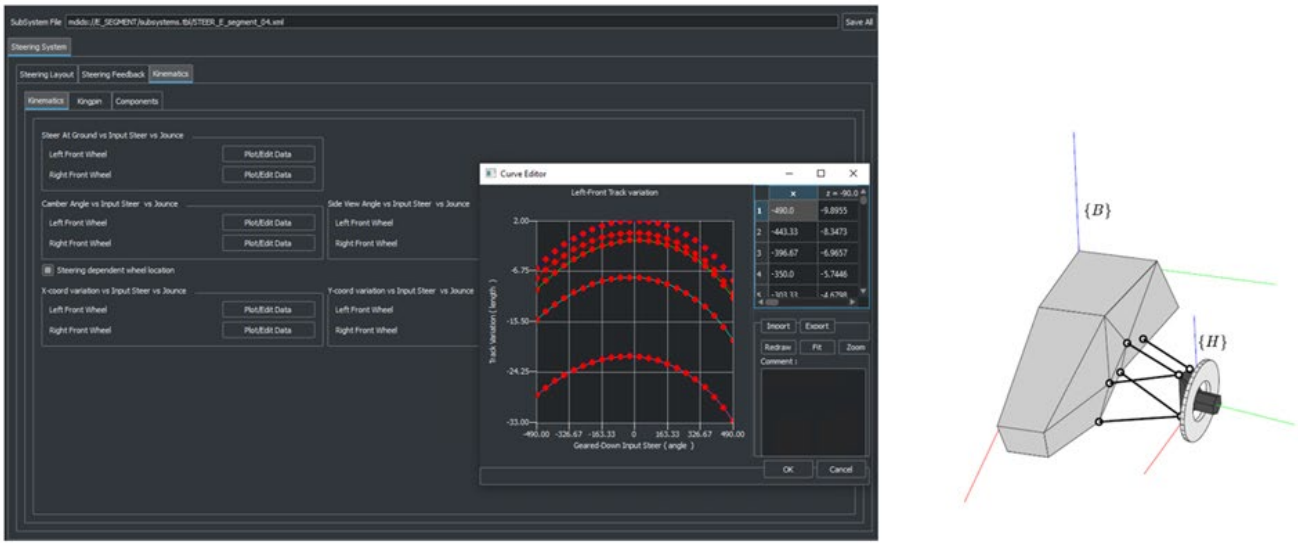

Figure 8: Suspension analysis

Tires.

The definition of tire forces requires construction of an auxiliary frame, with respect to which they are most naturally expressed. Once this frame is defined, the resultant tire force is decomposed along its axes. We distinguish between a vertical component, normal to ground, and a tangential one, tangent to the road plane.

The vertical force is computed using a compliant tire model, which also allows to correctly deal with the case that the tire loses contact with ground, e.g. during a jump. The tangential force is computed instead according to the well-known Magic Formula by Pacejka, implementing a PAC 2002 model.

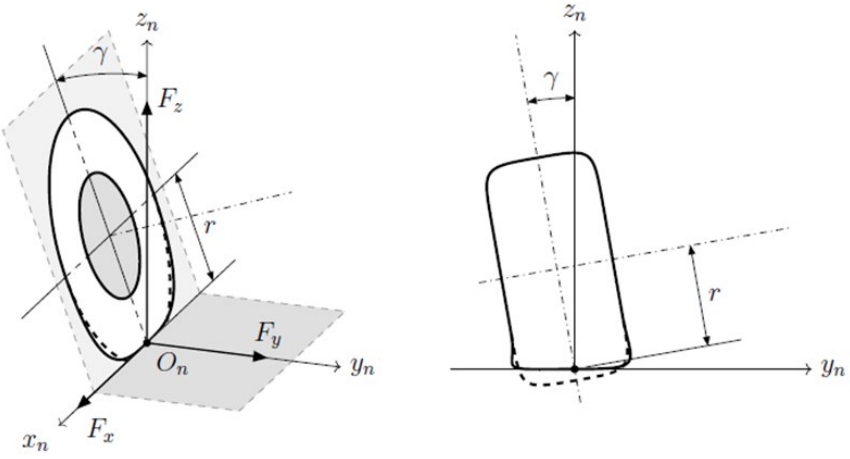

Figure 9: Decomposition of the tire force into normal and tangential components, and a detail on the vertical compliance.

Powertrain

The engine curve is implemented as a constant power curve set up to its maximum value.

Three different type of differential are implemented in our model: 1) Open, 2) LSD Torsen, 3) LSD with preload. The transmission is defined through a smoothed gear transition function, as shown in Figure 8.

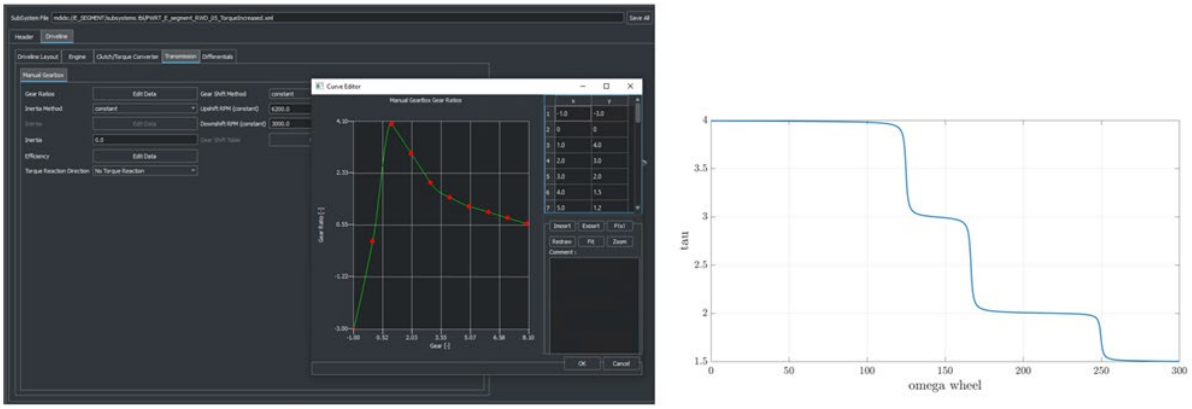

Figure 10: Transmission ratio.

External Forces.

Concerning the other external forces acting on the vehicle, there is the weight force on each body, and the aerodynamic forces (drag and downforce) generated by the chassis bodywork. We also included among the external forces the driving and braking torque applied to each wheel, together with their reactions.

To write the dynamical equations of our vehicle, we adapted the Articulated Body Algorithm (ABA) by Featherstone. The basic advantage of this approach (from both the computational and analytical point of view) is that, rather than writing the vehicle equations of motion explicitly - something that would be near to impossible to do by hand, unless large approximations are made to simplify the model - these are built recursively, so that one always has to deal with one rigid body at a time.

As far as the working of the ABA is concerned, the algorithm sees the mechanical system as a graph (in fact, a tree), where nodes are bodies and edges are joints. At each iteration, the algorithm goes through the graph and propagates quantities from body to body. There are three steps at each iteration:

1. In the first step, twist velocities are propagated forward across rigid bodies, from the chassis to the knuckles, and then to the rims;
2. In the second step, the articulated inertia and bias force of each body is computed, starting from the terminal bodies in the tree. According to Featherstone, the “articulated inertia" is the inertia that a body appears to have when it is part of an articulated system of bodies. The “articulated bias" instead, is defined as the value that the resultant wrench applied by the parent node on the tree should take in order for the body to have zero acceleration. If any external force acts on the body, then its contribution falls directly into the bias force. For a leaf node in the kinematic tree, the articulated inertia and bias are simply the generalized inertia matrix of the body of the bias force acting on it.
3. In the third and final step, the twist acceleration of the chassis is computed and then propagated forward to the terminal links of the tree. Joint accelerations will be retrieved in the process.

Data and Comparison

All the data required by our model is taken from the Model 1 (CarRealTime model).

Some simulations have been performed to compare the handwritten and the commercial model.

One of these simulations is the steering ramp shown in Figure 11.

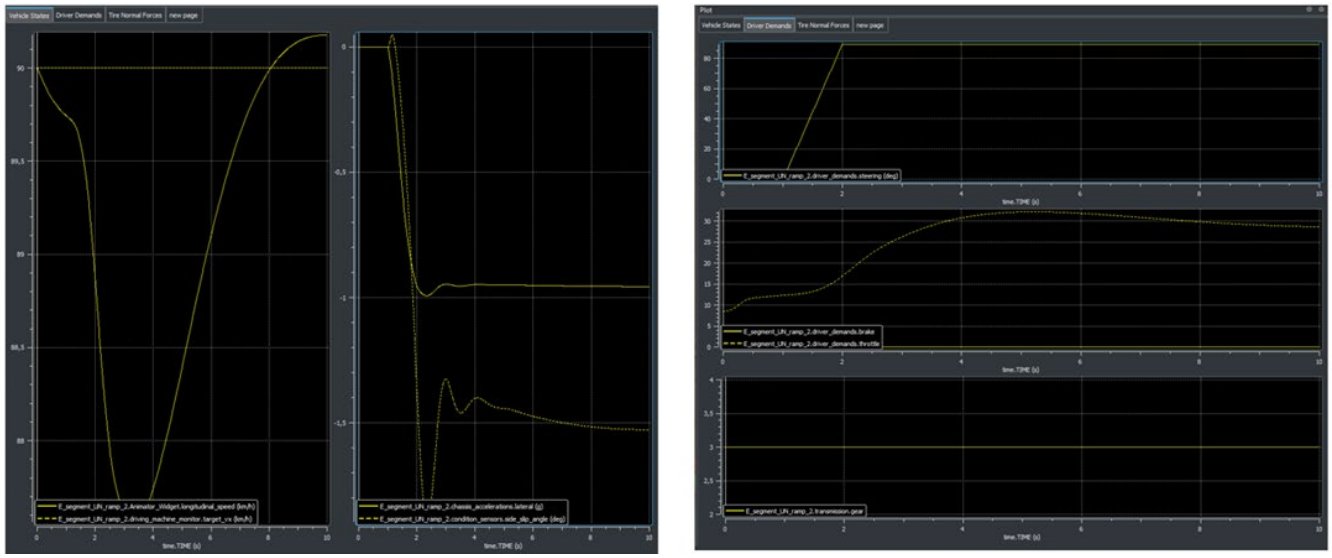

Figure 11: Control inputs for the steering ramp maneuver

The comparison has been conducted across vertical, lateral and longitudinal loads demonstrating strong agreement, as shown in Figure 12, Figure 13, and Figure 14.

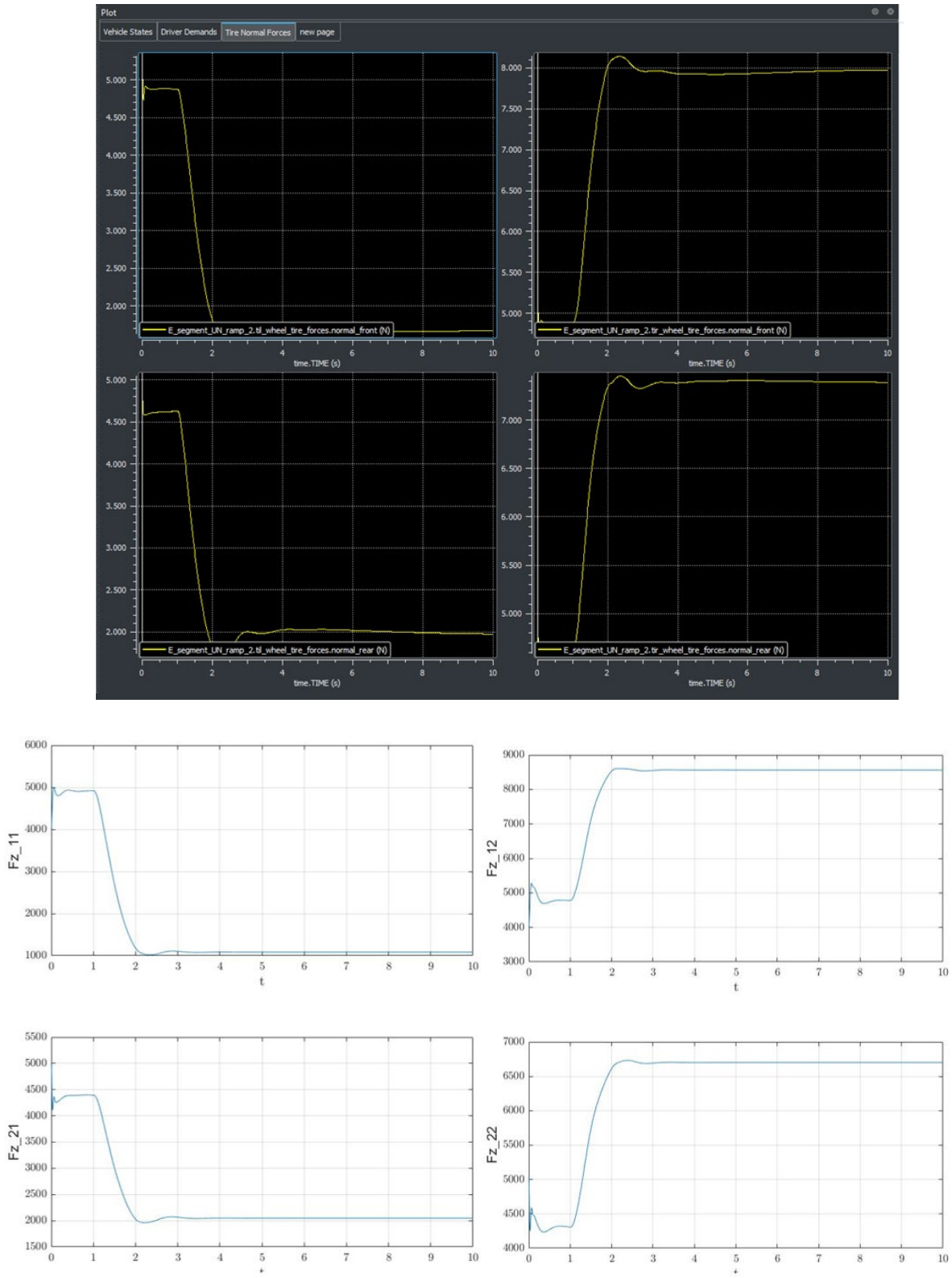

Figure 12: Comparison across vertical tire loads

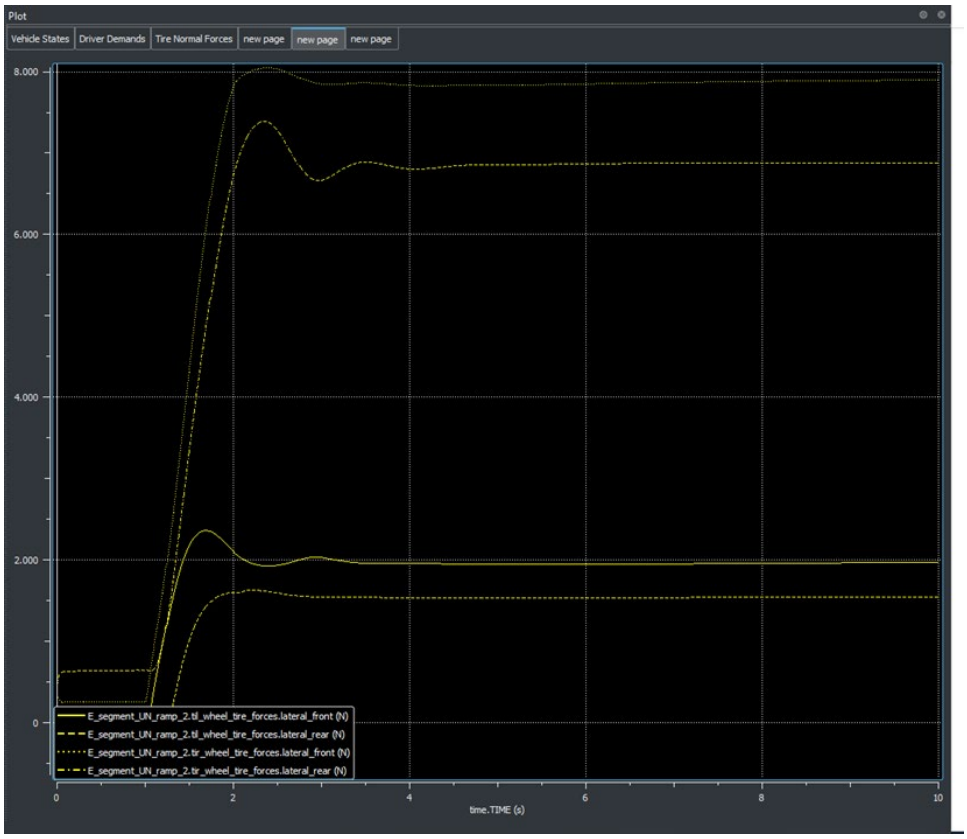

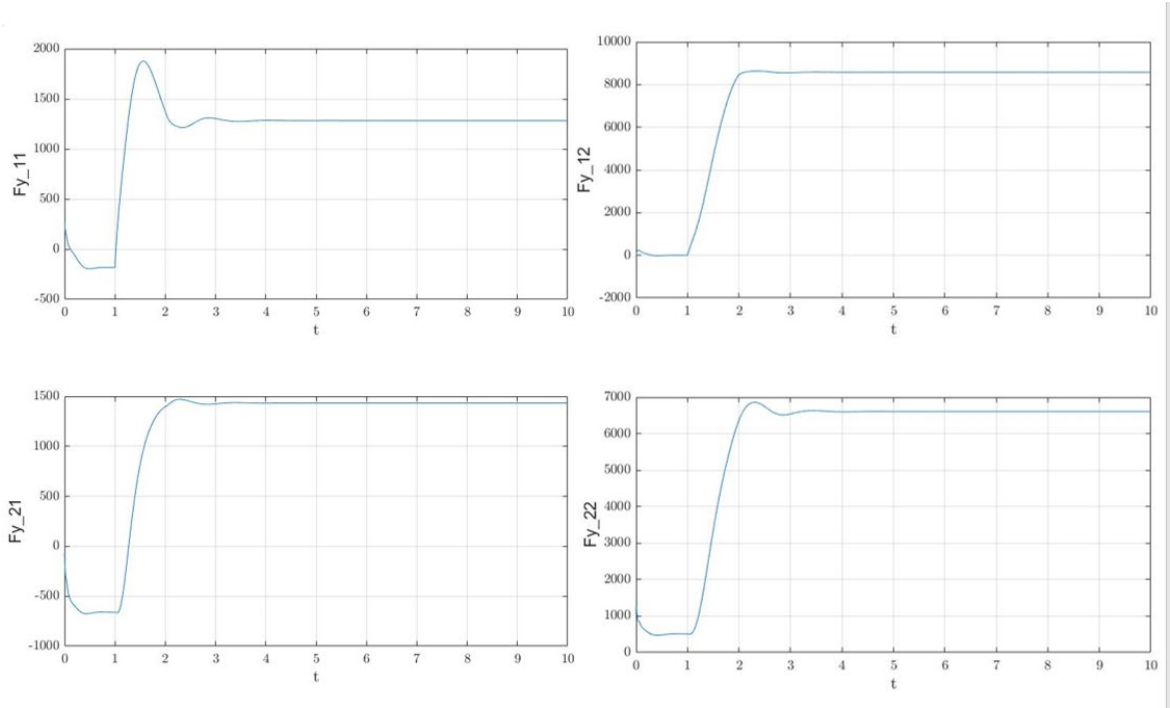

Figure 13: Comparison across lateral tire loads

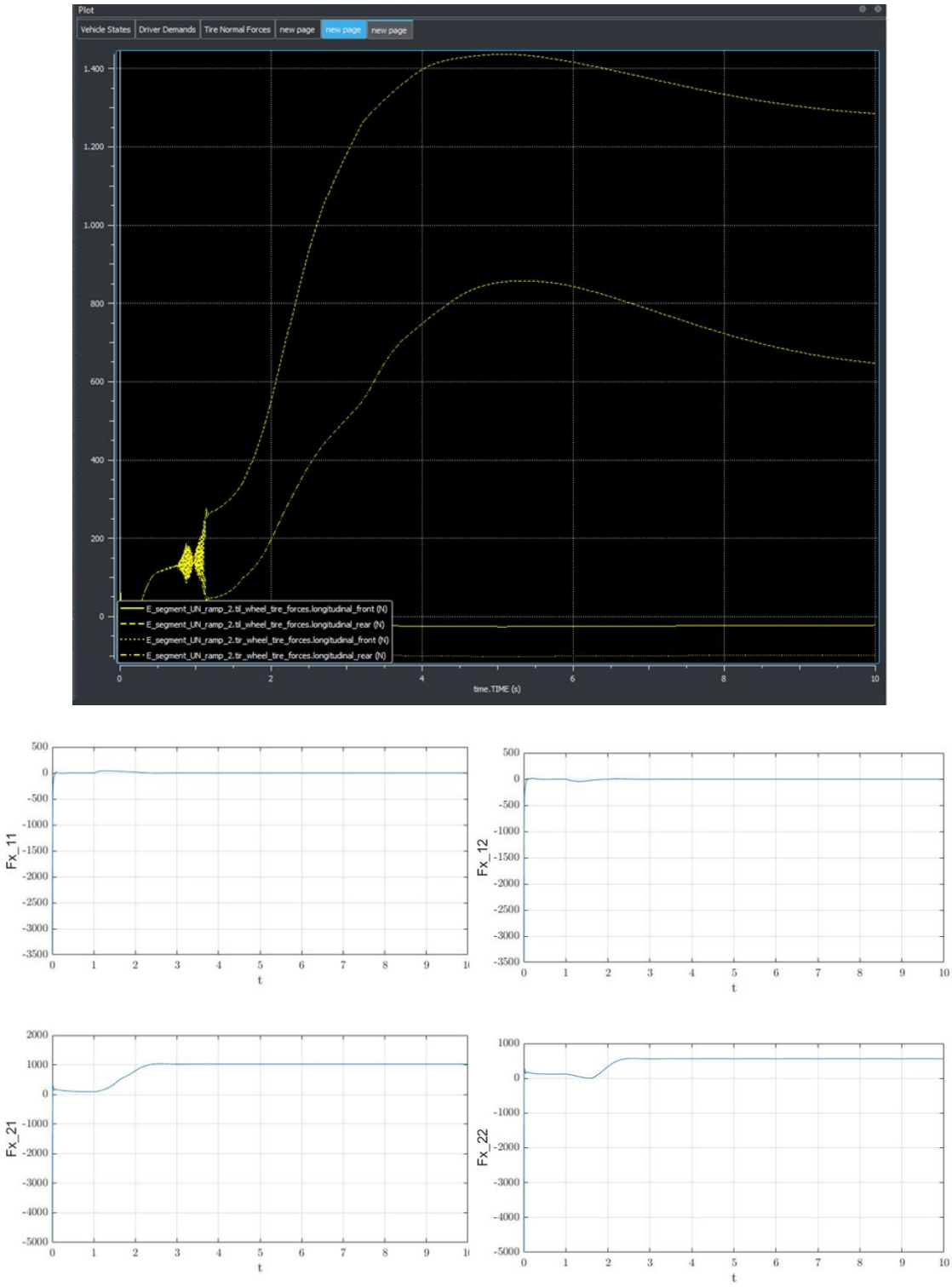

Figure 14: Comparison across longitudinal tire loads

2 Driver models

In this section, the driver models considered in the project are described.

2.1 Third-order delay driver model

The driver model is developed according to [5]. For the straight running of the vehicle, referring to the reference system of Figure 1, the task of the driver is to place the preview point *P* on the *X* axis, i.e. the y coordinate y_P of the point has to be equal to zero. For the task, the driver controls the steering wheel. The steering action is proportional to the path error computed at a certain distance in front of the vehicle. This distance *L* is proportional to the longitudinal speed *u* by setting a fixed preview time T_{prev}, so $L = T_{prev}\, u$. The coordinates of the preview point in the global reference system and its speed components can be computed starting from the coordinates of the center of gravity in the global reference system as follows

$$\boldsymbol{P} = (x_P)\boldsymbol{i_0} + (y_P)\boldsymbol{j_0} = (x_G + L\cos\psi)\boldsymbol{i_0} + (y_G + L\sin\psi)\boldsymbol{j_0}$$

Eq. 13

The speed of point P reads

$$\boldsymbol{V_P} = (\dot{x_P})\boldsymbol{i_0} + (\dot{y_P})\boldsymbol{j_0} = \left(\dot{x_G} - \dot{\psi}L\,sin\,\psi\right)\boldsymbol{i_0} + \left(\dot{y_G} + \dot{\psi}L\,cos\,\psi\right)\boldsymbol{j_0}$$

Eq. 14

The path error is

$$e = \left(y_{ref} - y_P\right) = -y_P = y_G - L\sin\psi$$

Eq. 15

$$\dot{e} = \left(\dot{y_{ref}} - \dot{y_P}\right) = -\dot{y_P}$$

Eq. 16

The steering angle is applied by the driver with a delay τ that, from the literature [5][6][7], is generally estimated to be 0.2s.

$$\delta(t+\tau) = ke(t) + k_d\dot{e}(t)$$

Eq. 17

A convenient Taylor approximation of Eq.10 in the neighbourhood of τ = 0.2s is

$$\delta(t+\tau) = \delta(t) + \dot{\delta}(t)\tau + \frac{1}{2}\ddot{\delta}(t)\tau^2 + \frac{1}{6}\dddot{\delta}(t)\tau^3$$

Eq. 18

One may easily check that the error due to such an approximation is very small in the range *0-2Hz* of steering angle frequency actuation.

As frequently defined in the literature [5], the time delay τ is 0.2s. The error is not acceptable for an expansion of Taylor's series lower than the third order. The fourth order and the Padé approximation work well but the added complexity has been reputed not balancing the increase of accuracy with respect to the third order Taylor's approximation.

The driver parameters are summarized in Table 4

Table 4: Driver parameters.

τ	0.2 s
k	0.01
k_d	0.008
T_{prev}	0.5 s

The model is available to all the researchers involved in the project, in the shared repository along with all pertinent data.

3 Control models

The overall system architecture is depicted in Figure 15. The basic principle of the control strategy is to generate a vehicle yaw torque M_z in response to deviations of the measured yaw rate (r) w.r.t. the reference one $(\bar{r})$. Such approach is a rather common paradigm for implementing vehicle dynamics controls also known as ESC, ESP, VDC etc.

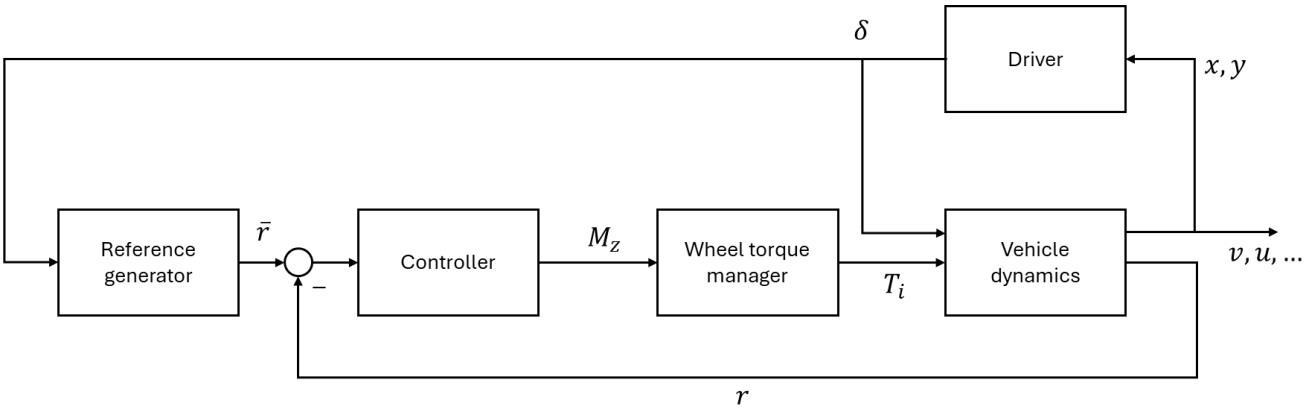

Figure 15. Block diagram of the overall vehicle dynamics control system.

The scheme comprises the following modules:

- Reference generator
- Controller
- Wheel torque manager
- Vehicle dynamics model, as described in Section 1.4.

In the following, the mathematical model of each block is discussed.

3.1 Reference generator

The reference generator produces the reference vehicle's yaw rate. It represents the expected (or the desired) vehicle dynamics behaviour, from the perspective of the driver steering input. The reference is typically computed by using the driver steering as input to the following static system:

$$\bar{r} = \frac{u}{l + k_{us}u^2}\delta$$

Eq. 19

where $l = l_f + l_r$ and k_{us} is the so called "understeering coefficient", that embeds the understeering $(k_{us} > 0)$, oversteering $(k_{us} < 0)$ or netural $(k_{us} = 0)$ vehicle behaviour.

More advanced implementations of the reference might include reference saturations as well as also some dynamics elements.

3.2 Controller

The controller computes the yaw moment in response to the measured yaw rate error. Such controller is typically a SISO (Single Input – Single Output) LTI (Linear Time Invariant) dynamic system, which can be described in terms of its transfer function $R(s)$.

A simple, yet effective, implementation typically exploits a simple proportional controller, where

$$R(s) = k_r$$

Eq. 20

The appeal of such a solution is that, beside the obvious minimum number of parameters, the lack of any dynamics makes the controller more robust w.r.t. the windup phenomena that can be induced by the wheel torque saturations (see the following section).

3.3 Wheel torque manager

The purpose of such component is toproperly assign the wheel torques (driving or braking) so to implement the desired vehicle yaw torque. The Wheel torque manager module is strongly affected by the vehicle powertrain architecture, for instance whether the system can act on each wheel independently assigning braking and traction torques or not.

A key point in the design of the torque allocator is the inclusion of the tire force saturations, due to the limited tire-road friction coefficient and the actual lateral force exerted by the tire. This problem is graphically well-described by so-called friction ellipse saturation diagram, sketched in the following Figure 16, that depicts the relationship between the maximum longitudinal (y-axis) and lateral (x-axis) force that the tire can exert.

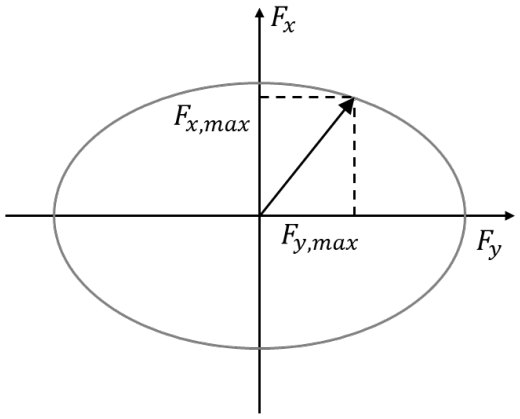

Figure 16. Friction ellipse saturation diagram sketch

In order to properly address such an issue, several implementations of the wheel torque manager block are possible, ranging from simpler open-loop and static solutions to complex feedback, to optimization-based ones.

At the present stage, simpler open-loop solutions have been considered. One solution is presented in the following, for an independent 4WD vehicle. Similar models will be developed for other vehicle powertrain configurations.

For the considered vehicle powertrain architecture, the wheel torque allocation manager

1. Applies to the left/right wheels equal and opposite torques
2. Evenly split the required yaw torque on the front/rear axles

In turn, the equations that implement the proposed Wheel torque manager are:

$$T_{fl} = sat\left[-\frac{M_z R_{fl}}{2p}\right]_{-f(\alpha_{fl})}^{f(\alpha_{fl})}$$

Eq. 21

$$T_{fr} = sat\left[\frac{M_z R_{fl}}{2p}\right]_{-f(\alpha_{fr})}^{f(\alpha_{fr})}$$

Eq. 22

$$T_{rl} = sat\left[-\frac{M_z R_{rl}}{2p}\right]_{-f(\alpha_{rl})}^{f(\alpha_{rl})}$$

Eq. 23

$$T_{rr} = sat\left[-\frac{M_z R_{rr}}{2p}\right]_{-f(\alpha_{rr})}^{f(\alpha_{rr})}$$

Eq. 24

The functions $f(\alpha_{fl}), f(\alpha_{fr}), f(\alpha_{rl}), f(\alpha_{rr})$ are derived from the Pacjeka formulas in a tire nominal conditions and are meant to avoid to exceed the wheel torque values that would go beyond the friction ellipse limits.

The proposed solution doesn't account for the following potential issues:

1. Due to tire saturations, the requested yaw torque could not be met and the overall control performance could degrade.
2. Due to changes in the road-friction coefficient, the *a-priori* imposed saturations could become inappropriate and lead to excessive wheel torque requests.

To overcome these limitations the following solutions could be implemented:

1. Explicitly include the saturation information within the Controller, relying on a more complex control strategy (to address issue 1)
2. Design a more complex wheel torque manager, for instance based on the solution of an optimization problem (to address issue 1)
3. Design on a low-level controller (i.e. an ABS and TC control) that limits the wheel torque based on the real-time feedback of the tire longitudinal slip (to address issue 2)

4 Measurement of vehicle parameters

This section is devoted to the description of the measurement systems for the measurement of the tyre characteristics and of the inertia properties of vehicles.

4.1 Measurement of the tyre characteristics

The Moving Laboratory for Automotive components Safety (MoLAS) assessment has been used for the tyres mechanical characterisation.

MoLAS is able to characterize tire sizes ranging from 16 to 24 inches. Tire forces are measured by means of a 6-axis measuring wheel mounted on the spindle. The measuring wheel was designed and realized at Politecnico di Milano and allows the real-time measure of the three forces and moments acting at the tire-terrain interface.

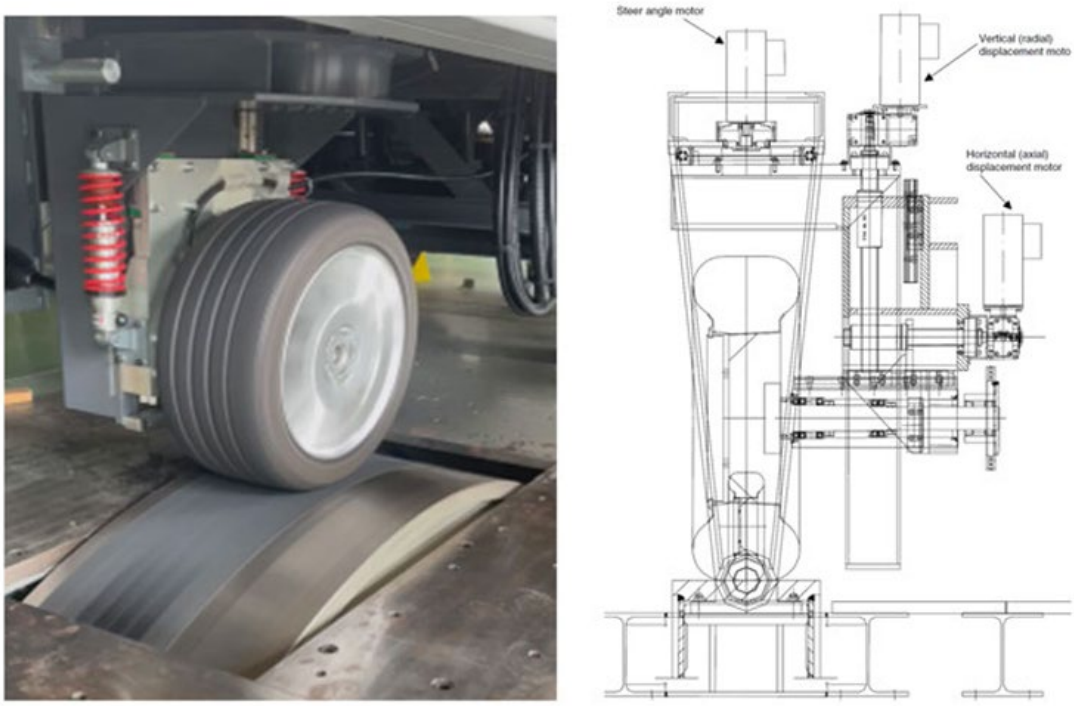

Figure 17. Tyre under testing.

The wheel is connected to the supporting structure by means of a double stage suspension system designed to filter out vertical disturbances coming from road irregularity. The vertical load is imposed by means of a pneumatic spring placed on top of the wheel supporting structure. The camber angle is imposed by means of an electro-mechanical linear actuator mounted on top of the rotating frame; the wheel camber angle can be varied in the range ±5◦. The steering angle is enforced by means of a second electric motor mounted on the steering axis. An electromagnetic retarder is used to apply and control the braking torque. Contact forces and moments acting at the tire-road interface are measured by means of the six-axis dynamometric wheel (main specification in the following table).

	Value	Units
Maximum force	15000	N
Maximum moment	4500	Nm
Accuracy (95%)	±5%	[-]
Cross-talk	< 1%	[-]
CAN bus communication speed	1	Mbps
Latency	13	ms

Figure 18. Six axis force sensor specification.

The tyre was inflated at 210 kPa and tested at different load combinations. The drum tangential speed was set to 22.2 m/s, a series of tests in pure lateral, pure longitudinal and combined lateral-longitudinal conditions have been conducted. The drum surface was covered with a specific sandpaper tape to increase the tire-surface friction coefficient replicating high grip dry asphalt conditions.

Three different levels of nominal vertical loads were set for the tests, namely 2900 N, 4000 N and 5200 N. The lateral force was applied by imposing a steering motion law in the range ±10◦ following the triangular waveform.

The acquired data were used for characterizing the tire behavior under pure cornering, pure longitudinal and combined slip conditions. Experimental samples have employed in a curve fitting procedure to identify the MF parameters. In the processing stage, data were accurately selected, cut, phased and filtered in order to remove noise, disturbances and recover the small latency due to the wireless transmission of the wheel force sensor.

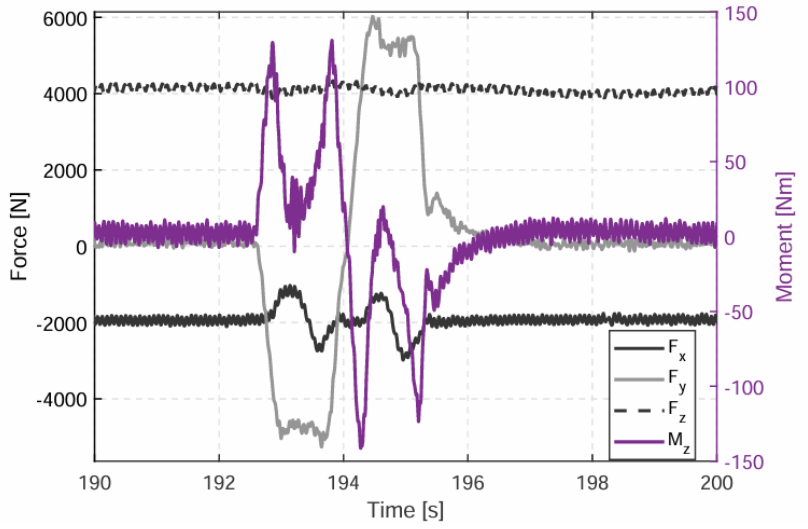

Figure 19. Acquired signals three tyre forces and self-aligning moment.

The set of the MF model coefficients identified by means of the tire modelling tool implemented in Adams Car. This tool outputs the result of the fitting process in a tire property file (*.tir), which contains all the information regarding the tire behavior under the possible operative conditions.

4.2 Measurement of the inertia parameters

For the measurement of the inertia parameters of vehicles, namely mass, centre of mass location and inertia tensor, at Politecnico di Milano the InTenso+ System is available [8]. The test rigs based on this measurement method are basically multi-bar pendulum carrying the body under investigation.

In Figure 20 the two test rigs currently available are shown. The larger version (Left), named InTenso+, has been used for full car vehicles and light farm tractors, while the other one, named InTensino+ (Right), has been used for engines, gearboxes, and small artificial satellites.

Figure 20: InTenso+ System for the measurement of the inertia parameters. Left: InTenso+ test rig for rigid bodies up to 3500 kg. Right: InTensino+ test rig for relatively light and compact rigid bodies (up to 400 kg).

The test rigs are composed of a frame for carrying a rigid body, four (or three) bars connecting this frame to another external frame fixed near the ceiling of the laboratory. The bars are connected to the 'ceiling frame' and to the 'carrying frame' by low-friction spherical joints, each one composed of a Hooke's joint (fitted with roller bearings) and an axial ball bearing. For both test rigs the natural frequencies have been measured at full load and they are above 10 Hz.

The measurement is performed by displacing the multi-bar pendulum carrying the body under investigation from rest. The following complex motion is recorded by means of encoders and load cells. By knowing the motion of the system and the forces along the bars, the inertia properties of the body are derived by a proper mathematical procedure (see for more details). A deformable multibody model is employed in the identification procedure to take into account the (small) deformation of the system. Aerodynamic drag during the motion of the pendulum can be considered in case vehicles are equipped with aerodynamic surfaces (i.e. racing cars [9]).

The specifications of the test rigs are reported in Table 5.

Details on the calibration and verification procedures can be found in [8],[9].

The inertia parameters of the reference vehicle are reported in Table 1.

Table 5: Technical specification of the InTenso+ and InTensino+ test rigs.

Test rig	InTenso+	InTensino+
Payload range [kg]	500 – 3500	50 – 400
Maximum dimensions of the body (LxWxH) [m]	7x2x1.6(*)	3x1x1(*)
Motion frequency [Hz]	< 5	< 5
Peak acceleration during test (min.-max) [m/s2]	2-10	3-10
CG uncertainty (in plane, height) [mm]	± 3 - ± 5	± 1.5 - ± 3
Moment of inertia (MOI) uncertainty	± 1%	± 1%
POI accuracy (% of the maximum MOI of the body)	± 0.5%	± 0.5%
MOI and POI resolution (% of the maximum MOI of the body)	0.2 %	0.2 %
Testing time [minutes](**)	< 10	< 10

(*) Dimensions are indicative. Fully customised fixturing can be realized.
(**) The testing time does not consider the time needed to position the body on the test rig.

5 Track and driving simulator tests

The 14dof-com model has been previously validated. In this deliverable, we refer to a session of track tests focused on the estimation of the actraction basin of the vehicle. The Maserati Ghibli used for the definition and previous validation of the model has been used for the tests and it is depicted in Figure 21. The car was fully instrumented with IMU, steering angle sensor and GPS. All of the ADAS and Stability enhancement systems (ABS, ESC, TCS) were removed. The tests were performed on dry track asphalt.

Figure 21: Car used to validate the vehicle models.

A distub to the straight motion of the car has been applied by a special control connected to the steering wheel able to generate a sinusoidal disturbance. For an example of a sinusoidal disturbance see Figure 22. The driver was instructed to drive straight ahead until the pre-defined speed was reached, then, the automatic sinusoidal steering was activated. Immediately after the sinusoidal steering was completed, the driver tried to recover the straight motion.

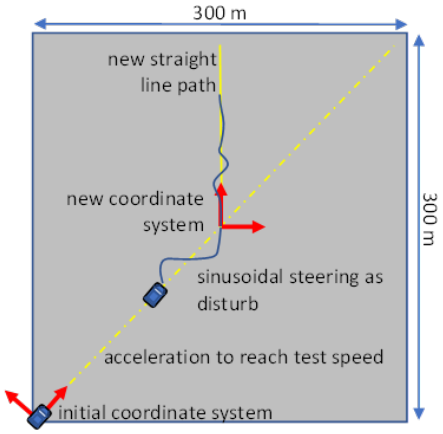

Figure 22: Tests on track. Square surface on which tests were performed. The driver did try to follow a straight line after the sinusoidal steering disturbance did act.

The sinusoidal steering did produce a disturbance on several states. Precisely, v, r, yG, and $\dot{y_G}$ were particularly affected by the disturbance. Due to this occurrence, a special test procedure was designed in order to focus on v and r only as disturbances. The only disturbed states had to be v and r, as they are the most relevant for the definition of the basin of actraction. The relevance of v and r states has been introduced above, the reader may understand why our attention has been devoted to v and r . In Figure 22 the scheme of the manoeuver is shown. After the sinusoidal steering action has produced a disturbed motion, the driver tries to run straight ahead along a new linear path. This allows to avoid the disturbance effects of both yG,

and $\dot{y}_G$. This way the only disturbance comes from v and r. The recovery action was successful or not, depending on v and r values. The manouvre has been repeated on the driving simulator of Politecnico di Milano by employing the 14dof-com model.

By inspection of Figure 23, it appears that the initial conditions that induce an unstable motion are similar for the driving simulator (14dof-com model), for the considered simple model (2dof model + 3rd-order delay driver model), and for the track. The same occurs for stable motions. From these tests, the models considered for the project appear to be able to predict the basin of attraction of the considered vehicle.

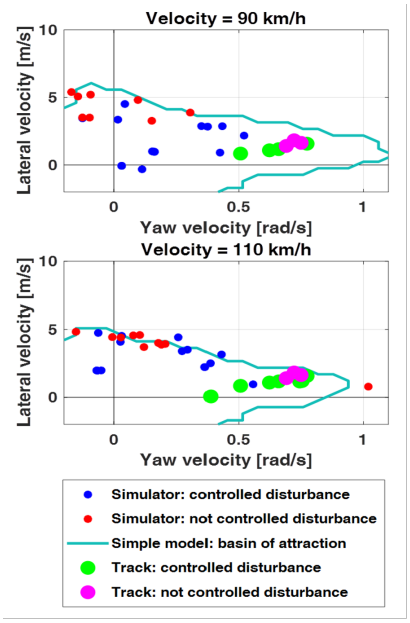

Figure 23: Tests on track. Just a portion of the basin of attraction is shown. Small dots refer to tests at the driving simulator, big dots refer to the tests on track. The employed models are the 2dof model (simple model) and the 14dof-com model (simulator model)

6 Published documents

The following table summarizes the published documents pertinent to the project.

Table 6: Published documents pertinent to the project.

1. Mastinu, G., Previati, G., Della Rossa, F., Gobbi, M. et al., "How Drivers Lose Control of the Car," SAE Int. J. Veh. Dyn., Stab., and NVH 8(1):99-121, 2024, doi:10.4271/10-08-01-0007
2. Mastinu, G., Previati, G., Della Rossa, F., Gobbi, M. et al., "How Drivers Lose Control of the Car," SAE WCX Congress, Detroit, 18 April 2024.
3. Giacintucci, S., Della Rossa, F., Mastinu, G., Previati, G., Gobbi, M.,Time delay effects on vehicle-and-driver stability, TDS, Udine September 2024
4. Mastinu, G., Previati, G., Gobbi, M., How limit cycles characterize car-and-driver motion, AVEC'24, Milan, September 2024
5. Gobbi, Massimiliano; Mastinu, Giampiero; Milivinti, Massimiliano; Previati, Giorgio, "Vehicle-and-driver stability analysis by a simple model and by a dynamic driving simulator", DSC 2024 EUROPE ^{VR} Driving Simulation Conference & Exhibition (Submitted)
6. Federico Maria Ballo, Alessio Biffi, Massimiliano Gobbi, Gianpiero Mastinu, "Advanced Tire Testing by an Innovative Moving Laboratory for Automotive Components Safety Assessment (Molas)", ASME IDETC-CIE 2024, Washington (Submitted)
7. Giacintucci, Samuele, "Global Stability of Road Vehicle and Driver", Graduate Thesis, Politecnico di Milano, Supervisor Gianpiero Mastinu, 2024

7 Conclusions

The present report fulfills Milestone 1 "Car and Driver models ready" of the STAVE project. The report describes the vehicle models employed for the project.

Five vehicle models with different levels of complexity have been selected. The most complex models can be employed in the driving simulator to include an actual human being in the analysis of the stability of the system vehicle plus driver. Simpler vehicle models will be used for the theoretical stability analysis and for the preliminary design of the control system of the vehicle.

A suitable driver model for the characterization of the driver is also described in the report. The chosen driver model features a third-order delay to correctly catch the effect of the driver on vehicle stability. Also, a control model is considered for the vehicle. The basic principle of the control strategy is to generate a vehicle yaw torque in response to deviations of the measured yaw rate with respect to the reference one.

Tyres characteristics and vehicle inertia parameters play a major role in the dynamic simulation of vehicle motion. In the report, the experimental methods employed at Politecnico di Milano are described. By using such methods, these parameters can be measured with a high level of accuracy. The experimental activity for the stability analysis of the vehicle is also described. The activity comprises both test at the driving simulator and on a track. The agreement between the tests is good.

Finally, a list of published documents pertinent to the project is provided.

References

[1] https://www.vi-grade.com/, retrieved February 2024.

[2] Pacejka, H.B., Tyre and Vehicle Dynamics. Butterworth and Heinemann (also SAE). Oxford, U.K., 2002, 2nd edn., 2006; 3ed., 2013

[3] Mastinu G, Biggio, D., Della Rossa, F., Fainello, M., Straight running stability of automobiles – experiments with a driving simulator, Nonlinear Dynamics, 99, pages 2801–2818(2020)

[4] Mastinu, G., Della Rossa, F., Previati, G. et al. Global stability of road vehicle motion with driver control. Nonlinear Dyn 111, 18043–18059 (2023). https://doi.org/10.1007/s11071-023-08794-z

[5] Plöchl, M., Edelmann, J., Driver models in automobile dynamics, Vehicle System Dynamics, Volume 45, Issue 7-8, July/August 2007, Pages 699-741

[6] Mastinu, G., Ploechl, M., (Eds). Road-and off-road Vehicle System Dynamics Handbook, CRC, Boca Raton, USA, 2014

[7] Mitschke, M, Wallentowitz, H., Dyanmik der Kraftfahrzeuge, Springer, Berlin, 2015

[8] M. Gobbi, G. Mastinu, and G. Previati, "A method for measuring the inertia properties of rigid bodies," *Mech. Syst. Signal Process.*, vol. 25, no. 1, pp. 305–318, Jan. 2011

[9] G. Previati, M. Gobbi, and G. Mastinu, "Method for the Measurement of the Inertia Properties of Bodies with Aerofoils," *J. Aircr.*, vol. 49, no. 2, pp. 444–452, Mar. 2012.